A Binary Shaped Mask Coronagraph for a Segmented Pupil

Keigo Enya

Department of Infrared Astrophysics, Institute of Space and Astronautical Science,

Japan Aerospace Exploration Agency Yoshinodai 3-1-1, Sagamihara, Kanagawa 229-8510

enya@ir.isas.jaxa.jp

and

Lyu Abe

Laboratoire Hippolyte Fizeau UMR 6525 Université de Nice-Sophia Antipolis Parc Valrose, F-06108

Nice, France

Lyu.Abe@unice.fr

Abstract

We present the concept of a binary shaped mask coronagraph applicable to a telescope pupil including obscuration, based on previous works on binary shaped pupil mask by Kasdin et al. (2005) and Vanderbei (1999). Solutions with multi-barcode masks which "skip over" the obscuration are shown for various types of pupil of telescope, such as SUBARU, JWST, SPICA, and other examples. The number of diffraction tails in the point spread function of the coronagraphic image is reduced to two, thus offering a large discovery angle. The concept of mask rotation is also presented, which allows post-processing removal of diffraction tails and provides a 360° continuous discovery angle. It is suggested that the presented concept offers solutions which potentially allow large telescopes with segmented pupil in future to be used as platforms for an coronagraph.

Key words: instrumentation: high angular resolution—telescopes—stars: planetary systems

1. Introduction

Direct detection and spectroscopy of extra-solar planets (hereafter exo-planets) is expected to be one of essential methods in the understanding of the manner in which planetary systems are born, how they evolve, and, ultimately, the identification of biological signatures on these planets. The enormous contrast in luminosity between a central star and an associated

planet has been a critical difficulty in the direct observation of exo-planets. For instance, if the solar system is suposed to be observed from outside, the contrast of luminosity between the Sun and Earth is 10^{-10} at visible light wavelengths and 10^{-6} in the mid-infrared wavelength region (Traub & Jucks 2002). Therefore, the number of exo-planets detected directly is somewhat smaller than those detected by other methods (Mayor & Queloz 1995; Charbonneau et al. 2000), although the first direct observation has been finally achieved (Marois et al. 2008; Kalas et al. 2008). The coronagraph, which was first developed for solar observation (Lyot 1939), is a special optics designed to reduce contrast. It is considered that a coronagraph, designed to achieve a very high dynamic range has the potential to further extend the possibility of the direct observation of exo-planets.

It has been considered that the performance of the coronagraph is decreased by obscuration in the telescope pupil which occurs from the secondary mirror, its support structure and the gaps between segmented mirrors. For example, in the case of a checkerboard coronagraph (Vanderbei, Kasdin, & Spergel 2004), which is a type of binary pupil mask coronagraph, the inner working angle (IWA), with and without obscuration by the secondary mirror, is $3\lambda/D$ and $7\lambda/D$ respectively, where λ is the wavelength and D is the diameter of the aperture (Tanaka et al. 2006; Enya et al. 2007). In fact, off-axis telescopes are considered for proposed future space missions specializing in coronagraphy, e.g., TPF-C (Traub et al. 2006); SEE-COAST(Schneider et al. 2006); PECO (Guyon et al. 2009), in order to avoid pupil obscuration. And therefore, various coronagraphs have been presented (e.g., summary in Guyon et al. 2006) for pupils without obscuration. If a reduction in the influence of pupil obscuration in the coronagraph design is possible, the value of on-axis telescopes for general purposes (current working telescopes and those under construction) as platforms for a coronagraph becomes much higher.

This paper presents a concept of solutions to realize a coronagraph for a segmented pupil by employing a binary shaped pupil mask.

2. Concept of Multi-barcode Mask Solution

Among the various current coronagraphic methods, coronagraphs using binary shaped pupil masks have some advantages in principle. Essentially the function of a binary pupil mask coronagraph to produce high contrast point spread function (PSF) is achromatic (except effect of scaling of PSF size), and is somewhat less sensitive to telescope pointing error than experienced with other coronagraphs (e.g., Lyot 1939). Another important property of binary pupil mask coronagraphs is the fact that they use only part of the pupil as the transmissive area of the mask. In this work, we employ this property to obtain solutions in coronagraph design with binary masks which "skip over" the obscured part of the pupil.

Fig. 1 shows an example of a solution for a segmented telescope pupil. In this case, the pupil is obscured by the secondary mirror and four off-center support structures, similar to the pupil of the SUBARU and GEMINI telescopes, as shown in the top panel of Fig. 1. The bottom

left panel shows the coronagraphic PSF expected from the pupil mask. Two dark regions, DR1 and DR2, are produced in the PSF. It must be noted that the principle of this coronagraph is essentially the same as that of the one-dimensional coronagraph by barcode mask presented by Kasdin et al.(2005), while the length of the barcode mask in the vertical direction in Fig. 1 is finite, and the barcode is split into two sets (i.e., double barcode mask), above and below the obstruction created by the secondary mirror. This solution has a coronagraphic power only in the horizontal direction. LOQO, a software presented by Vanderbei (1990), was used to optimize each barcode mask. IWA, the outer working angle (OWA), and the contrast (C_0) required for optimization of a one-dimensional coronagraph were $3.0\lambda/D$, $16\lambda/D$, and better than 10^{-5}, respectively. In this work, the throughput is simply defined as the ratio of the area of transmission of the pupil, with and without the pupil mask, which is equivalent to the ratio of the areas of the white and black regions in the figure. The throughput for the solution shown in Fig. 1 is 24%. Values of IWA, OWA, C_0, and the throughput is summarized in Table 4, together with values of other solutions described below. The central obstruction of this solution against the coronagraph is determined by the width of the support structure, which is much smaller than the diameter of the obstruction due to the secondary mirror. As a result, a smaller IWA is realized. This solution has no coronagraphic power in the vertical direction. Along the vertical direction, the intensity of the PSF decreases, following the diffraction theory applied to a rectangular aperture, and there is no OWA. Therefore, the contrast defined as the intensity ratio between the core of the PSF and each position in the dark region, C, is not constant (C is better than, or equal to C_0).

3. Solutions for Various Pupils

3.1. Pupil Resulting from Hexagonal Mirrors

The top of Fig. 2 shows a solution using an off-centered four barcode mask applied to a segmented telescope pupil, consisting of hexagonal mirrors and obstructions created by a secondary mirror and its support structure. This type of design of telescope is adopted by the James Webb Space Telescope (JWST). IWA, OWA, and C_0 in this solution are $3.5\lambda/D_{hex}$, $19\lambda/D_{hex}$, and $10^{-5.0}$, respectively, in which D_{hex} is defined as shown in Fig. 2. The throughput of the solution is 24%. Off-centering the barcode mask gives rise to a peculiar shape of the core of the PSF, while DR1 and DR2 values produced in this solution are similar to those when the barcode mask is not off-centered.

JWST carries coronagraphs in two instruments, the Near-Infrared Camera (NIRCAM) (Rieke et al. 2005; Green et al. 2005) and the Mid-Infrared Instrument (MIRI) (Boccaletti et al. 2007), in which Lyot-type coronagraphs and coronagraphs using four quadrant phase masks will be used. In these coronagraphs, the PSF is impaired by a complex diffraction pattern, especially by six bright tails in a radial direction from the core of the PSF resulting from the

segmentation of the pupil. As a result, the discovery angle of these coronagraphs is reduced, particularly in positions close to the core of the PSF. These coronagraphs use devices set at the focal plane in order to realize a high contrast image (i.e., at the occluting mask or four quadrant phase mask), so that these coronagraphs are, in principle, sensitive to telescope pointing error and have limited working bandwidth. If it is possible to use a binary pupil mask coronagraph, these limits are essentially relaxed and the discovery angle of the coronagraphic image can be improved. On the other hand, a solution using a binary pupil mask, as shown in Fig. 2, applies a constraint of OWA. In order to get the best coronagraph design for each mission, it is essential to estimate the expected observational performance from both the instrument specification and scientific simulation.

3.2. Pupil with Central Obscuration and On-axis Spiders

The bottom of Fig. 2 shows a solution provided by a double barcode mask, applied to an on-axis telescope pupil with obscuration by the secondary mirror and its four on-axis support structures. This is an example of a solution obtained from optimization presuming a central obstruction of the barcode mask. It should be noted that the central obstruction in this case is caused by the width of the support structure (not by the diameter of the secondary mirror). IWA, OWA, and C_0 in this solution are $3.4\lambda/D_{hex}$, $15\lambda/D_{hex}$, and $10^{-5.0}$, respectively. The throughput of the solution is 15%.

C and IWA of this solution satisfy the requirement for a mid-infrared coronagraph (Enya et al. 2010) for the Space Infrared telescope for Cosmology and Astrophysics (SPICA) (Nakagawa et al. 2009). SPICA will carry an on-axis Ritchey-Chretien telescope with a 3m class diameter aperture, and it is planned to be launched in 2018. Use of a binary-shaped pupil mask is considered as the baseline solution for the SPICA coronagraph because of its achromatic work, robustness against telescope pointing error caused by vibration of cryo-coolers and other mechanics, and feasibility.

3.3. Further Variations

Fig. 4 shows further variations of solutions consisting of multi barcode masks. Mask-4 is a solution for a telescope pupil which is the same as the pupil in the case of Mask-2. Four barcode masks used in Mask-4 and Mask-2 are common. In addition, four segments of the pupil, located to the left and right of the central obscuration, are used in order to demonstrate the improvement in the throughput. IWA, OWA, and C_0 in this solution are $3.9\lambda/D_{hex}$, $14\lambda/D_{hex}$, and $10^{-5.0}$, respectively. The throughput of this solution is 27%. Optimization of these newly used segments was carried out with the constraint of central obscuration, as in the case of Mask-3. In comparison with Mask-2, this solution can be regarded as an example in which C_0 is maintained but IWA and OWA is compromised as the result of trade-off.

Mask-5 is a solution for a telescope pupil which is same as the pupil in the case of Mask-3. Eight barcode masks were employed in order to extend the effective area used by masks.

Optimizations of each mask were carried out with constraints in the central obscuration caused by the secondary mirror or its support structure. IWA, OWA, and C_0 in this solution are $3.3\lambda/D$, 10λ, and $10^{-5.3}$, respectively. The throughput of this solution is 30%, implying a large improvement over the case of Mask-3. In comparison with Mask-3, this solution can be regarded as an example in which IWA is maintained but C_0 and OWA is compromised as the result of trade-off.

Further improvement in performance is possible, if the telescope design takes account of use of a multi-barcode pupil mask coronagraph. Mask-6 and Mask-7 are solutions presuming segmented rectangular mirrors. The throughput of these solutions are 50%, which is the highest of the solutions presented in this paper. For Mask-6, IWA, OWA, and C_0 in this solution are $3.6\lambda/D_{rect}$, $11\lambda/D_{rect}$, and $10^{-6.0}$, respectively, in which D_{rect} is defined as shown in Fig. 3. Mask-7 provides $IWA=2.5\lambda/D_{rect}$, which is significantly better than Mask-6, while C_0 and OWA are common to Mask-6 and Mask-7.

4.   Discussion and Summary

If rotation of the pupil mask and coronagraphic imaging, before and after the rotation, are possible, the total discovery angle is improved. Fig. 4 shows the concept of rotating the pupil mask by 90 degrees, applied to the solution shown in Fig. 2. As a result of double coronagraphic imaging, before and after mask rotation, most of the influence of the diffraction tails in the coronagraphic PSF is removed, and totally $360°$ continuous discovery angle is provided. The improved discovery angle makes it possible to observe companions of a central star, even if the companions are buried in diffraction tails of the original PSF. The mask rotation technique can be especially useful for SPICA, in which the role of the telescope (Trauger & Traub 2007) is strongly constrained due to the thermal system design required to realize a cryogenic infrared telescope satellite utilizing radiation cooling.

A binary shaped pupil mask has also been used in order to support a Phase Induced Amplitude Apodization (PIAA) coronagraph (Guyon et al. 2010). It is, in principle, possible with such a hybrid coronagraph to realize smaller IWA and higher throughput than the values in coronagraph employing only a binary shaped pupil mask. The currently presented hybrid coronagraph by Guyon et al. (2010) includes circular apodization produced by PIAA and a binary shaped mask consisting of concentric rings (Vanderbei, Kasdin, & Spergel 2003). Therefore, the coronagraphic power is along radial direction in PSF and is not one-dimensional. We would like to point out the potential to combine barcode masks and a one-dimensional PIAA in order to realize a one-dimensional hybrid coronagraph which is applicable to segmented telescope pupils like those shown in this paper.

In general, the size of a telescope aperture is limited by various factors. For instance, the size of the rocket fairing constrains off-axis space telescopes with seamless mirrors proposed especially for the observation of exo-planets. If a segmented pupil becomes more useful for

coronagraphic observation of exo-planets, on-axis telescopes with a segmented pupil for general purposes becomes more valuable as a coronagraph platform. In the case of ground based telescopes, the current largest class of telescopes (e.g. VLT, KECK, GEMINI, SUBARU and so on), can be good target for application of a one-dimensional coronagraph using a binary shaped mask. These telescopes are starting direct detections of giant, young planetary objects in near infrared (Chauvin et al. 2004; Marois et al. 2008; Lagrange et al. 2010; Thalmann et al. 2010). Giant ground based telescope of the futre (e.g., TMT, EELT) will extend these observations in spatial resolution and sensitivity.

Space telescopes have further potential, especially for observation in mid-infrared wavelength region. The contrast provided by several of solutions presented in this paper is $\sim 10^{-6}$, which is the contrast needed for observation of matured terrestrial exo-planets in the mid-infrared (Traub & Jucks 2002). This fact suggests that a mid-infrared coronagraph with giant telescope, consisting of segmented mirrors, has the potential for terrestrial planet search in future, where there is a critical spectral feature, O_3 (9.8μm) considered to be a biomarker in atmosphere of terrestrial planets. In contrast, coronagraphic search for terrestrial planets in the visible wavelength requires observation with much higher contrast, 10^{-10} (Traub & Jucks 2002), which any of the masks in this paper are unable to reach. Proposed off-axis telescopes with a seamless pupil, e.g., TPF-C (Traub et al. 2006); SEE-COAST (Schneider et al. 2006); PECO (Guyon et al. 2009) might be a reasonable solution to attain such ultimate contrast, rather than larger telescopes with a segmented pupil.

This paper presents a one-dimensional coronagraphic solution for a segmented telescope pupil by applying a type of binary shaped mask, a multiple barcode masks, which "skip over" the obscured part of the pupil. These coronagraphs have the general advantage of binary pupil mask coronagraphs, i.e., lack of susceptibility to telescope pointing errors and less constraint on the bandwidth. Furthermore, the multi-barcode mask coronagraph provides a large discovery angle and a small IWA, even for a pupil with a large central obstruction. We suggest that the concept of these solutions has a potential use in facilitating large telescopes having a segmented pupil to be used as platforms for an advanced coronagraph.

References

Boccaletti, A., Baudoz, P., Baudrand, J., Reess, J. M., & Rouan, D. 2005, Advances in Space Research, 36, 1099

Charbonneau, D., Brown, T. M., Latham, D. W., & Mayor, M. 2000, ApJL, 529, 45

Chauvin, G., Lagrange, A.-M., Dumas, C., Zuckerman, B., Mouillet, D., Song, I., Beuzit, J.-L., & Lowrance, P. 2004, A&A, 425, L29

Enya, K., & SPICA working group 2010, Advances in Space Research, 45, 979

Enya, K., Tanaka, S., Abe, L., & Nakagawa, T. 2007, A&A, 461, 783

Green, J. J., Beichman, C., Basinger, S. A., Horner, S., Meyer, M., Redding, D. C., Rieke, M., & Trauger, J. T. 2005, Proc. SPIE, 5905, 185

Guyon, O., Pluzhnik, E., Martinache, F., Totems, J., Tanaka, S., Matsuo, T., Blain, C., & Belikov, R. 2010, PASP, 122, 71

Guyon, O. et al. 2009, Proc. SPIE, 7440, 74400F

Guyon, O., Pluzhnik, E. A., Kuchner, M. J., Collins, B., & Ridgway, S. T. ApJS, 167, 81-99, 2006

Kalas, P., Graham, J. R., Chiang, E., Fitzgerald, M. P., & Clampin, M. 2008, Science, 322, 1345

Kasdin, N. J., Vanderbei, R. J., Littman, M. G. & Spergel, D. N. 2005, Appl. Opt., 44, 1117

Lagrange, A.-M., Bonnefoy, M., Chauvin, G., Apai, D., Ehrenreich, D., Boccaletti, A., Gratadour, D., Rouan, D., Mouillet, D., Lacour, S., & Kasper, M. 2010, Science, 329, 57

Lyot, B. 1939, MNRAS, 99, 580

Marois, C., Macintosh, B., Barman, T., Zuckerman, B., Song, I., Patience, J., Lafrenière, D., & Doyon, R. 2008, Science, 322, 1348

Mayor, M., & Queloz, D. 1995, Nature, 378, 355

Nakagawa, T., & Spica Team 2009, SPICA joint European/Japanese Workshop, held 6-8 July, 2009 at Oxford, United Kingdom. Edited by A. M. Heras, B. M. Swinyard, K. G. Isaak, and J. R. Goicoechea. EDP Sciences, 2009, p.01001

Rieke, M. J., Kelly, D., & Horner, S. 2005, Proc. SPIE, 5904, 1

Schneider, J. et al. 2006, Proceedings of the Annual meeting of the French Society of Astronomy and Astrophysics Eds.: D. Barret, F. Casoli, G. Lagache, A. Lecavelier, L. Pagani, p.429

Tanaka, S., Enya, K., Nakagawa, T., Kataza, H., & Abe, L. 2006, PASJ, 58, 627

Thalmann, C. et al. 2010, ApJL, 718, 87

Traub, W. A. et al. 2006, Proc. SPIE, 6268, 62680T-1

Traub, W. A., & Jucks, K. W. 2002, Astro-ph/0205369

Trauger, J. T., & Traub, W. A. 2007, Nature, 446, 771

Vanderbei, R. J., Kasdin, N. J. & Spergel, D. N. 2004, ApJ, 615, 555

Vanderbei, R. J., Kasdin, N. J. & Spergel, D. N. 2003, ApJ, 590, 593

Vanderbei, R. J. 1999, Optimization methods and software, 11, 451

Table 1. Parameters in mask designs.

Mask	C_0	IWA	OWA	Throughput (%)
Mask-1	$10^{-5.0}$	$3.0\,\lambda/D$	$16\,\lambda/D$	24
Mask-2	$10^{-5.0}$	$3.5\,\lambda/D_{hex}$	$19\,\lambda/D_{hex}$	24
Mask-3	$10^{-6.0}$	$3.4\,\lambda/D$	$15\,\lambda/D$	15
Mask-4	$10^{-5.0}$	$3.9\,\lambda/D_{hex}$	$14\,\lambda/D_{hex}$	27
Mask-5	$10^{-5.3}$	$3.3\,\lambda/D$	$10\,\lambda/D$	30
Mask-6	$10^{-6.0}$	$3.6\,\lambda/D_{rect}$	$11\,\lambda/D_{rect}$	50
Mask-7	$10^{-6.0}$	$2.5\,\lambda/D_{rect}$	$11\,\lambda/D_{rect}$	50
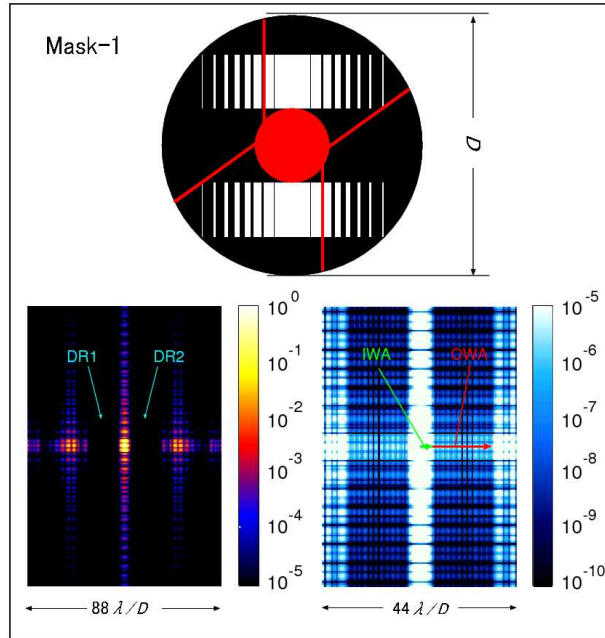
Fig. 1. Top: double barcode masks (white area) applied to the pupil of a telescope with a circular primary mirror (corresponding to black circle) with obscuration (red area). Transmissivity of the white and other areas (black and red) is 100% and 0%, respectively. Bottom: PSF derived from simulation using the mask above.
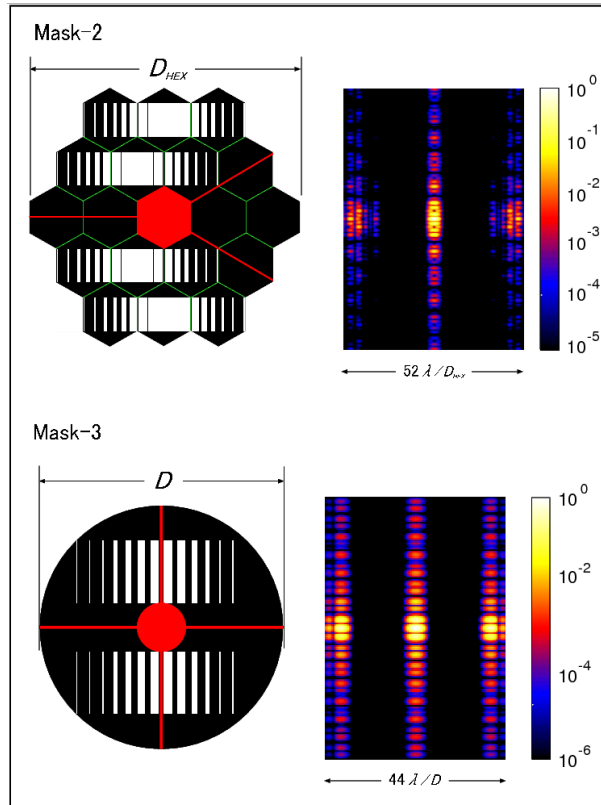
Fig. 2. Multi barcode masks and PSF derived from simulation. The green line in the Mask-2 shows the join between segments.
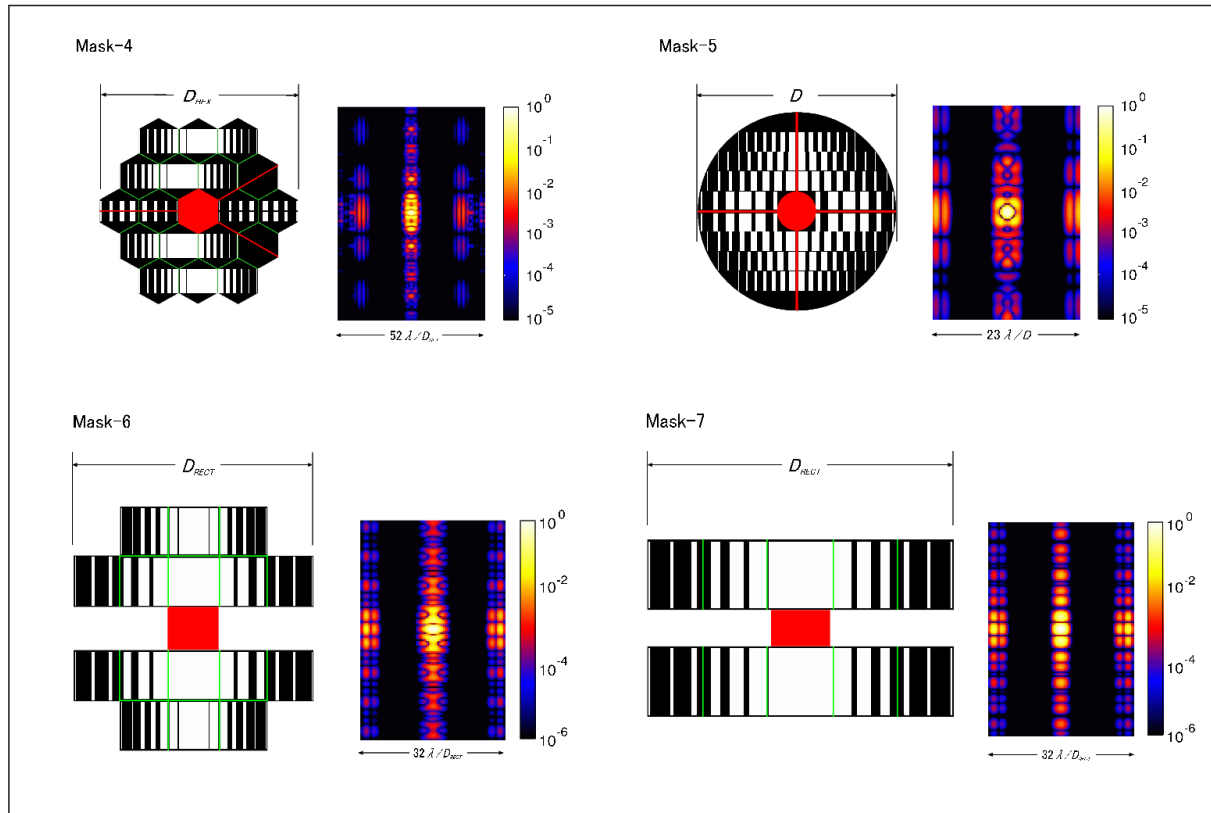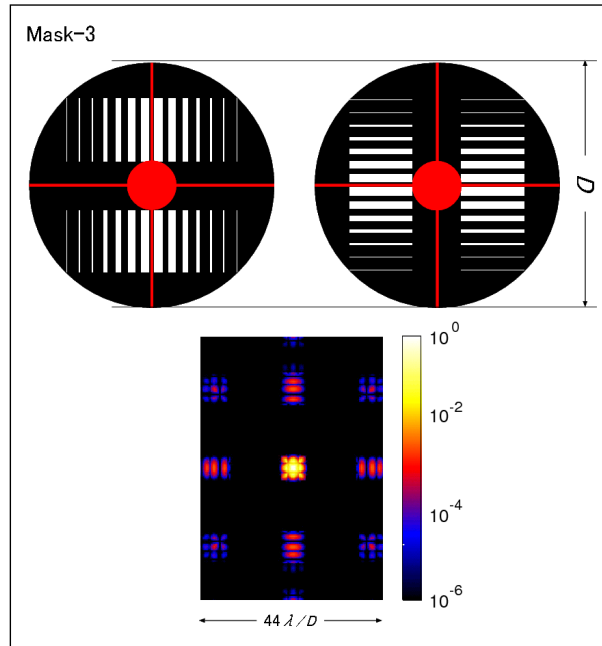
Fig. 3. Multi barcode masks and PSF derived from simulation.

Fig. 4. Concept of mask rotation. Top: mask configuration, before and after the rotation. Bottom: composite PSF, having a dark region as the sum of each of the dark regions of PSF, before and after the mask rotation.